

# Nonadiabatic excited-state molecular dynamics: Numerical tests of convergence and parameters

Tammie Nelson,<sup>1</sup> Sebastian Fernandez-Alberti,<sup>2</sup> Vladimir Chernyak,<sup>3</sup> Adrian E. Roitberg,<sup>4</sup> and Sergei Tretiak<sup>1,a)</sup>

<sup>1</sup>*Theoretical Division, Center for Nonlinear Studies (CNLS), and Center for Integrated Nanotechnologies (CINT), Los Alamos National Laboratory, Los Alamos, New Mexico 87545, USA*

<sup>2</sup>*Universidad Nacional de Quilmes, Roque Saenz Peña 352, B1876BXD Bernal, Argentina*

<sup>3</sup>*Department of Chemistry, Wayne State University, 5101 Cass Avenue, Detroit, Michigan 48202, USA*

<sup>4</sup>*Departments of Physics and Chemistry, Quantum Theory Project, University of Florida, Gainesville, Florida 32611, USA*

(Received 29 September 2011; accepted 11 January 2012; published online 3 February 2012)

Nonadiabatic molecular dynamics simulations, involving multiple Born-Oppenheimer potential energy surfaces, often require a large number of independent trajectories in order to achieve the desired convergence of the results, and simulation relies on different parameters that should be tested and compared. In addition to influencing the speed of the simulation, the chosen parameters combined with the frequently reduced number of trajectories can sometimes lead to unanticipated changes in the accuracy of the simulated dynamics. We have previously developed a nonadiabatic excited state molecular dynamics methodology employing Tully's fewest switches surface hopping algorithm. In this study, we seek to investigate the impact of the number of trajectories and the various parameters on the simulation of the photoinduced dynamics of distyrylbenzene (a small oligomer of polyphenylene vinylene) within our developed framework. Various user-defined parameters are analyzed: classical and quantum integration time steps, the value of the friction coefficient for Langevin dynamics, and the initial seed used for stochastic thermostat and hopping algorithms. Common approximations such as reduced number of nonadiabatic coupling terms and the classical path approximation are also investigated. Our analysis shows that, at least for the considered molecular system, a minimum of  $\sim 400$  independent trajectories should be calculated in order to achieve statistical averaging necessary for convergence of the calculated relaxation timescales. © 2012 American Institute of Physics. [doi:10.1063/1.3680565]

## I. INTRODUCTION

The simulation of nonadiabatic molecular dynamics (NA-MD) has rapidly become an indispensable tool for understanding complex ultra-fast photophysical processes such as charge and energy transfer, and non-radiative relaxation.<sup>1–13</sup> Computational modeling is truly a complement to experiment: it often provides mechanistic information that cannot be detected through measurement alone or serves as a powerful predictive tool to stimulate new research. With the development of femtosecond spectroscopy techniques, methods for the simulation of nonadiabatic dynamics have advanced<sup>14,15</sup> to meet the demand. Molecular dynamics with quantum transitions (MDQT) is a well tested and computationally tractable surface hopping method for the simulation of nonadiabatic dynamics. In MDQT, quantum transitions are incorporated according to the fewest switches surface hopping (FSSH) stochastic algorithm described by Tully.<sup>16</sup> This scheme has become one of the most popular alternatives to Ehrenfest dynamics<sup>17</sup> due to its simplicity and accuracy especially in cases where mean-field approaches fail to capture the correct dynamics.<sup>18–20</sup>

MDQT and other varieties of surface hopping methods have been applied to a broad range of systems concerning different kinds of processes such as electronic coupling within simple theoretical models,<sup>21–25</sup> reactive scattering,<sup>26–28</sup> photodissociation of small molecules,<sup>29–31</sup> vibrational relaxation in clusters and condensed phase,<sup>32</sup> proton and electron transfer,<sup>33–35</sup> and photoexcitation of organic molecules.<sup>9–13</sup> Nevertheless, the stability of MDQT results to changes in parameters and the number of trajectories has been extensively analyzed only for the simplest models, while the robustness of the method applied to larger systems has received relatively little attention.<sup>36</sup>

A generalized framework for MDQT simulations of photoinduced dynamics in large organic molecules involving multiple coupled electronic excited states requires an “on-the-fly”<sup>37,38</sup> calculation of energies, gradients, and nonadiabatic coupling terms (NACTs). Efficient computation of these quantities represents one of the major bottlenecks in the field of theoretical simulations of organic photochemistry. Frequently, numerical expense precludes applications of sophisticated excited state *ab initio* methodologies to very large molecular systems requiring many trajectories and detailed sampling of conformational space to reach convergence. In a recent article,<sup>39</sup> we have presented a novel nonadiabatic excited state molecular dynamics (NA-ESMD)

<sup>a)</sup> Author to whom correspondence should be addressed. Electronic mail: serg@lanl.gov.

implementation that provides a computationally accessible and reasonably accurate description of photoinduced dynamics in large molecular systems consisting of hundreds of atoms on timescales on the order of tens of picoseconds. The method uses actual excited state potential energy surfaces and accounts for a minimal amount of many-body effects in the excited state [i.e., configuration interaction singles (CIS) or time-dependent Hartree-Fock (TDHF) approximation]. As a compromise, utilization of semiempirical model Hamiltonians delivers superb computational efficiency. The method has recently been successfully applied to model the photoinduced dynamics of conjugated distyrylbenzene (a short oligomer of polyphenylene vinylene, PPV)<sup>39</sup> and several small phenylene-ethynylene dendritic segments.<sup>8,40</sup> Such NA-ESMD simulations are possible due to “on the fly” calculations of excited state energies,<sup>41–43</sup> gradients,<sup>39,44,45</sup> and nonadiabatic coupling terms<sup>39,46–48</sup> analytically.

The two main obstacles in any MDQT simulation applied to real polyatomic molecules in condensed phase are the computational cost of each individual trajectory and the large ensemble of trajectories explicitly required. Compared to a single trajectory approach, the numerical cost of computing multiple trajectories needed for statistical averaging can be prohibitively expensive.<sup>49,50</sup> Nevertheless, individual trajectories are independent and propagation of a “swarm” of trajectories is trivially parallelizable to run computations on multiple processors.

Our NA-ESMD method<sup>39</sup> combines MDQT using the fewest switches criterion and Langevin dynamics algorithms; both are stochastic by nature. The stochastic behaviour is simulated through the use of a random number generator. A different random seed should be used for each independent trajectory, since trajectories with identical seeds starting from different geometries tend to synchronize over long simulation times.<sup>51</sup> The standard MDQT procedure consists of propagating a swarm of trajectories starting at different initial conditions and different random seeds. Therefore, the effect of random seeds on the overall dynamics of the ensemble should be addressed. That is, the extent to which the observed dynamics of the statistical average depends on the initial random seed assignment.

NA-MD simulations involve the simultaneous propagation of quantum electronic coefficients and classical nuclear coordinates. The quantum integration time step is usually required to be smaller than the classical time step used to integrate the nuclear equations of motion. Therefore, NACTs must be obtained at many intermediate times. This task is usually overcome by using simple linear interpolation and extrapolation schemes.<sup>21,36</sup> However, the NACTs are usually sharp peaks strongly localized in time, a feature that can introduce large inaccuracies in the interpolation approximation. Our recently developed NA-ESMD framework introduces flexibility by allowing NACTs to be evaluated a desired number of times during the interval between classical time steps. A comparison of the relative performance of both procedures remains to be evaluated since the optimum combination of quantum and classical integration time steps can have a large effect on the overall efficiency and accuracy of the calculations. These parameters should depend on each individual system, and sim-

ilar behavior should be expected within the same family of molecules.

Another aspect to be addressed in NA-MD simulations is the effective number of NACTs computed during the simulation. For a simulation involving  $N_S$  electronic states, there are  $N_S(N_S - 1)/2$  non-redundant coupling terms to be computed. The complete set of coupling terms is required for the exact integration of the equation of motion for the electronic wave function. In a complete coupling (CC) picture, all of the NACTs are computed. Various cutting schemes have been proposed in order to reduce the computational cost associated with evaluating the nonadiabatic coupling terms.<sup>52</sup> In these approximations, only a fraction of the  $N_S(N_S - 1)/2$  nonadiabatic coupling terms are computed at each integration time step. However, these schemes invariably introduce error in the propagation of the electronic wave function. In one such approximation, known as the partial coupling (PC) scheme, the coupling between states other than the current state is neglected, i.e., only coupling terms involving the current state are computed, and the number of coupling terms is significantly reduced to  $N_S - 1$ . A more severe approximation assumes that population will only flow from the current state to the state directly below in energy. This two-state (TS) model requires evaluation of only one coupling term and upward hops to higher energy are ignored.<sup>53</sup> Recent advances in analytic techniques have helped to mitigate the computational load of the coupling term<sup>39,46–48</sup> so that cutting schemes are not needed.

In addition to the NACT cutting schemes described above, various other approximations are often used to lighten the computational load of NA-MD routines.<sup>6,7,20,54</sup> The classical-path approximation (CPA) is a severe simplification which assumes that nuclear dynamics is independent of the electronic evolution, thereby circumventing the so-called quantum back-reaction problem. This allows a single nuclear trajectory, obtained for the ground electronic state, to be used to describe the nonadiabatic dynamics following photoexcitation. In this sense, nuclear evolution is given *a priori*. The CPA is only valid in cases where the forces imparted on the nuclei change little as the electronic subsystem evolves. Recent advances in the computation of excited state gradients practically eliminates the need for such approximations; the actual excited-state forces due to the quantum subsystem can be calculated analytically.<sup>41,44,45</sup>

Another issue that should be analyzed is the dissipation effects on the dynamics with use of a Langevin dynamics scheme within our NA-ESMD framework. A larger empirical friction coefficient  $\gamma$  potentially leads to faster vibrational relaxation. The resulting vibrational damping can reduce the value of the computed NACTs<sup>55</sup> with the concomitant effects on the electronic relaxation. Additionally, the choice of the friction coefficient can significantly impact the rate of conformational sampling in the system. This has been noted in previous protein folding simulations in which the dynamics were either accelerated or decelerated according to the frictional force.<sup>56,57</sup> In the MDQT approach, preparation of the initial conditions is a critical preliminary step in the simulations. The initial sampling of conformational space (before any electronic excitation takes place) should be adequate to represent

the equilibrated ensemble of molecules at given thermodynamic conditions. Typically, this requires computing a long Born-Oppenheimer (BO) ground state trajectory of the system with parameters (temperature  $T$  and friction coefficient  $\gamma$ ) consistent with the future excited state simulations. Therefore, the minimum time required to achieve the adequate ground state conformational sampling should be evaluated.

In this article, we extend our previous work to study the effects that the number of trajectories and various parameters have on the NA-ESMD simulation of distyrylbenzene. Various user-defined parameters are analyzed: classical and quantum integration time steps, the number of nonadiabatic coupling terms to be considered, the value of the friction coefficient for Langevin dynamics, and the initial seed used for stochastic thermostat and hopping algorithm. Our analysis demonstrates the flexibility and robustness of the NA-ESMD framework to variation of any of these parameters.

Section II provides a brief description of the theoretical approach used in our simulations including a discussion of the Langevin equation of motion and the implementation of the surface hopping methodology. The results of our numerical simulations of photoexcited dynamics in distyrylbenzene are presented in Sec. III including a detailed analysis of the tested parameters such as optimum integration time steps, the number of trajectories used for statistical averaging, and the random number seed. Calculation of NACTs and NACT cutting schemes are also discussed, and the validity of the classical-path approximation is analyzed. Finally, the impact of the friction coefficient for Langevin dynamics is investigated with special consideration for the effect on ground state conformational sampling. Our findings are summarized in Sec. IV.

## II. THEORETICAL METHODOLOGY

The NA-ESMD model combines the FSSH algorithm, as it is used in the MDQT method,<sup>16,21</sup> with “on the fly” calculation of the electronic energies, gradients, and nonadiabatic coupling vectors for the excited states using a collective electronic oscillator (CEO) package.<sup>41,58–60</sup> The CEO code is based on well-tested semiempirical models combined with the TDHF or the CIS formalism to describe correlated excited states. A detailed description of the CEO code and NA-ESMD implementation can be found elsewhere.<sup>39,41,49</sup>

MDQT treats the electronic degrees of freedom quantum mechanically, while the motion of the nuclei is treated classically. A swarm of  $N$  classical trajectories is propagated constituting a photoexcited wavepacket. The nuclei of each trajectory are evolved on a single adiabatic potential energy surface (PES) rather than in the mean field, and transitions between coupled electronic states are possible depending on the strength of the NACTs. In our NA-ESMD implementation, the electronic wave function is expanded in terms of the adiabatic many-electron basis functions  $\phi_\alpha(\mathbf{r}; \mathbf{R}(t))$  (CIS or TDHF approximation), representing a mixed state

$$\Psi(\mathbf{r}, \mathbf{R}, t) = \sum_{\alpha} c_{\alpha}(t) \phi_{\alpha}(\mathbf{r}; \mathbf{R}(t)), \quad (1)$$

where the time-dependent expansion coefficients are given by  $c_{\alpha}(t)$ , while  $\mathbf{r}$  and  $\mathbf{R}$  are the electronic and nuclear degrees of

freedom, respectively. Substitution of Eq. (1) into the time-dependent Schrödinger equation yields the equation of motion for the coefficients  $c_{\alpha}(t)$ ,

$$i\hbar \frac{\partial c_{\alpha}(t)}{\partial t} = c_{\alpha}(t) E_{\alpha} - i\hbar \sum_{\beta \neq \alpha} c_{\beta}(t) \dot{\mathbf{R}} \cdot \mathbf{d}_{\alpha\beta}, \quad (2)$$

where the equation has been simplified by expressing the adiabatic basis functions  $\{\phi_{\alpha}\}$  as eigenstates of the Hamiltonian.  $\mathbf{d}_{\alpha\beta}$  is known as the nonadiabatic coupling vector and is defined as

$$\mathbf{d}_{\alpha\beta} = \langle \phi_{\alpha}(\mathbf{R}) | \nabla_{\mathbf{R}} \phi_{\beta}(\mathbf{R}) \rangle \quad (3)$$

and  $\dot{\mathbf{R}} \cdot \mathbf{d}_{\alpha\beta}$  is the scalar nonadiabatic coupling term (NACT) given by

$$\dot{\mathbf{R}} \cdot \mathbf{d}_{\alpha\beta} = \left\langle \phi_{\alpha} \left| \frac{\partial \phi_{\beta}}{\partial t} \right. \right\rangle, \quad (4)$$

where  $\dot{\mathbf{R}} = \partial \mathbf{R} / \partial t$ . Within the NA-ESMD framework, these quantities are calculated analytically.<sup>39,46,47</sup>

The nuclei are propagated using the Velocity Verlet<sup>61,62</sup> algorithm where the time step  $\Delta t$  is employed. A constant-temperature Langevin dynamics algorithm<sup>63</sup> with a friction coefficient  $\gamma$  ( $\text{ps}^{-1}$ ), developed to be consistent with the velocity Verlet integration technique, is implemented in the NA-ESMD framework. The Park-Miller “minimal standard” pseudo-random number generator<sup>64</sup> following numerical recipes<sup>65</sup> is used to determine both the stochastic force and to evaluate the acceptance/rejection of hops in the surface hopping algorithm. The variations of the quantum coefficients requires a smaller quantum time step  $\delta t \leq \Delta t$  where the number of quantum steps per classical integration step is given by  $N_q = \Delta t / \delta t$ . The time evolution of the coefficients in Eq. (2) can be split into real and imaginary parts yielding a system of coupled equations,<sup>39</sup> which can be solved using the Runge-Kutta-Verner fifth- and sixth-order method based on a code designed by Hull, Enright, and Jackson.<sup>66,67</sup> The excited state energies,  $E_{\alpha}(\mathbf{R})$ , and NACTs,  $\dot{\mathbf{R}} \cdot \mathbf{d}_{\alpha\beta}$ , are evaluated at intermediate times between classical time steps with  $\delta t$  time-interval. Meanwhile, the hopping probability is evaluated at each classical time step. While hops are attempted at each classical step, the transition probability is accumulated where a summation is performed over the contributions of each quantum step using the corresponding value of NACT for each of them.<sup>21,39</sup> The values of the nuclear coordinates at  $t + n\delta t$  are obtained using the Velocity Verlet equations with values of  $\dot{\mathbf{R}}_i$  and  $\mathbf{R}_i$  evaluated at  $t$ . Propagating classical and quantum equations with two different algorithms, as described in detail in Ref. 39, can be justified by the advantages and disadvantages of each.<sup>68</sup> Selecting the optimum combination of these integration parameters can have a large effect on the efficiency and accuracy of the simulations.

## III. NA-ESMD MODELING OF PHOTOINDUCED DYNAMICS IN DISTYRYLBENZENE

### A. Molecular dynamics simulations

The chemical structure of distyrylbenzene, a small oligomer of polyphenylene vinylene, is shown in Fig. 1. For

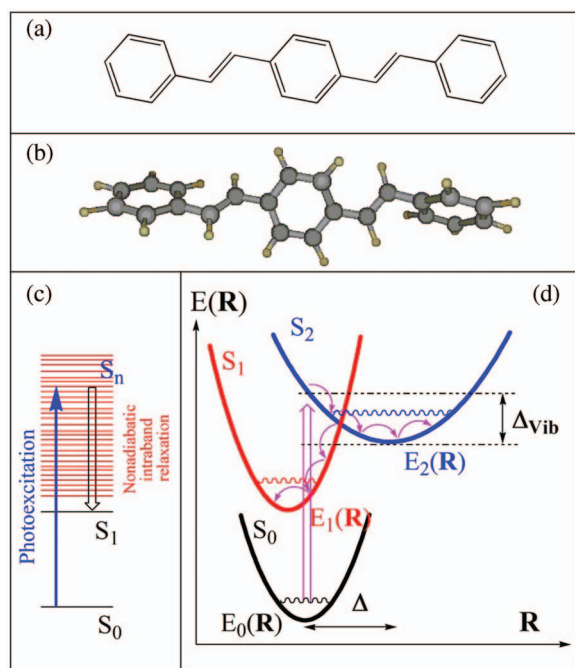


FIG. 1. (a) Chemical structure of distyrylbenzene and (b) a snapshot from the ground-state trajectory revealing the geometry conformations. (c) Schematic representation of molecular photoexcitation and intraband relaxation (internal conversion) via nonadiabatic vibronic dynamics. (d) Schematic representation of MDQT dynamics. The excited state energy  $E_\alpha$  is a function of the nuclear coordinates  $\mathbf{R}$ . The nuclear trajectory is propagated on the excited state Born-Oppenheimer potential energy surface and transitions between electronic states are allowed.

all simulations presented here, we use the AM1/CIS level of theory. Our first step is modeling of the photoinduced dynamics of distyrylbenzene at room temperature (300 K). We start by computing ground state molecular dynamics simulations consisting of six BO trajectories of 100 ps using the time step  $\Delta t = 0.5$  fs. The Langevin thermostat<sup>63</sup> was used to keep the temperature constant with a friction coefficient  $\gamma = 2.0$  ps<sup>-1</sup>. The system was heated and allowed to equilibrate to a final temperature of  $T_0 = 300$  K during the first 10 ps of each trajectory. The remainder of each trajectory was then used to collect a set of initial positions and momenta for the subsequent excited state simulations. Configurations were sampled with intervals of 0.5 ps for a total of 1080 initial configurations for the subsequent MDQT simulations in the excited states.

Nonadiabatic excited state trajectories were started from these initial configurations after a vertical excitation to the highly excited  $mA_g$  (or  $S_m$ ) state. The  $mA_g$  (or  $S_m$ ) transition is a significant state in conjugated polymers corresponding to a delocalized excitonic transition.<sup>69</sup> In experiment, photoexcited dynamics is typically studied by ultrafast pump-probe spectroscopy.<sup>70</sup> Experimentally determined absorption spectra for distyrylbenzene place the lowest excited state  $1B_u$  ( $S_1$ ) at 2.74 eV (calculated vertical transition energy is 3.1 eV) and the  $mA_g$  has a 1.72 eV separation from  $S_1$  (calculated value is 2.0 eV).<sup>69,71,72</sup> The ground state  $S_0$  has  $1A_g$  symmetry. As a consequence, the transition  $1A_g \rightarrow 1B_u$  is optically allowed, while the  $1A_g \rightarrow mA_g$  transition is forbidden. However, the  $mA_g$  state can be populated by the optically allowed  $1B_u \rightarrow mA_g$  transition.

Here, we focus on the intraband relaxation (see Fig. 1) as the system passes nonadiabatic regions and transitions between multiple BO surfaces. In order to determine the  $mA_g$  state, the 20 lowest excited states were calculated for each starting geometry and the transition with the highest oscillator strength from  $1B_u$  state was selected. We found that for the  $S_m$  state,  $m$  varied from 8 to 12 due to conformational disorder induced by thermal fluctuations at 300 K. Excited state trajectories were propagated for 1 ps at 300 K, and  $N_S = 15$  excited states were included in our simulations in order to allow transitions to higher energy states. Unless otherwise noted, the standard parameters used in the NA-ESMD simulations are  $\Delta t = 0.1$  fs,  $N_q = 3$ , and  $\gamma = 2.0$  ps<sup>-1</sup>, where 1080 independent trajectories are used. In order to compare the effects of the different tested parameters and approximations among the various simulations, the steady rise of the  $S_1$  state population was monitored by fitting the curve to the following empirical equation:

$$f(t) = \frac{A \exp(t/\tau^1)}{A + \exp(t/\tau^1)} - \frac{A}{1 + A}. \quad (5)$$

The timescale for the  $S_1$  population growth is given by  $\tau^1$  and  $A$  is a normalization constant which has been constrained to satisfy the criteria of  $f(0) = 0$  and  $f(\infty) = 1$  to provide physically relevant population analysis.

## B. Optimum set of parameters and convergence

### 1. Classical and quantum integration time steps

Evaluation of NACTs at intermediate times between two classical steps is required during the propagation of the quantum coefficients, and linear interpolation schemes<sup>21,36</sup> have been the standard procedure for this purpose. The validity range of the interpolated values introduces limitations to the size of the classical integration step for an accurate propagation of the nuclei. Our NA-ESMD framework introduces flexibility in the evaluation of NACTs by allowing them to be calculated a desired number of times *between* classical time steps. That is, the calculation of NACTs and excited-state gradients can be separated. In this way, larger classical time steps can be employed and the numerical expense for calculation of gradients can be reduced. However, this computational savings can potentially be negated if the number of quantum steps per classical step is too large causing an increase in the computational cost for several NACT calculations. Therefore, we have tested various combinations of classical time step  $\Delta t$  and number of quantum steps  $N_q$  in our NA-ESMD simulations of intraband relaxation in distyrylbenzene. The tested parameters as well as the associated normalized CPU time per trajectory are provided in Table I. For each combination of parameters, a total of 1080 independent trajectories have been calculated. The parameters  $\Delta t = 0.01$  fs and  $N_q = 10$  were chosen to represent the *accurate* “reference” case, while the other tested parameters range from  $\Delta t = 0.1$  to 2.0 fs with either 1, 3, or 5 quantum time steps per classical step. We note that our “reference” case does not necessarily provides fully numerically converged results by adequately exploring *every* NACT peak appearing upon state crossings for all

TABLE I. Classical ( $\Delta t$ ) and quantum ( $\delta t$ ) integration time step parameters for NA-ESMD simulations and a number of quantum steps per classical step ( $N_q$ ) along with normalized average CPU times per trajectory.

$\Delta t$ (fs)	$\delta t^a$ (fs)	$N_q$	CPU time
0.01	0.001	10	1.0
0.1	0.02	5	0.09
0.1	0.033	3	0.07
0.5	0.17	3	0.02
2.0	2.0	1	0.003

<sup>a</sup> $\delta t = \Delta t/N_q$ .

trajectories (see our discussion of Fig. 3). However, further reduction of the timestep parameters is impractical due to significant increase of numerical efforts (see Table I) and emerging dependence of the results on the convergence parameters for Davidson's algorithm used to obtain excited states via iterative scheme.<sup>39</sup> Indeed, even for all other equal parameters (initial conditions, time steps, etc.), two trajectories with different Davidson's convergence criteria diverge. This effect particularly escalates for small time steps below  $\Delta t = 0.01$  fs.

Figure 2 shows the population rise for the  $S_1$  state for each of the tested combinations of classical and quantum integration time steps. The top panel shows the results for the standard mA<sub>g</sub> relaxation dynamics using  $N_S = 15$  excited states and 1080 trajectories. The rapid decay of the initial  $S_m$

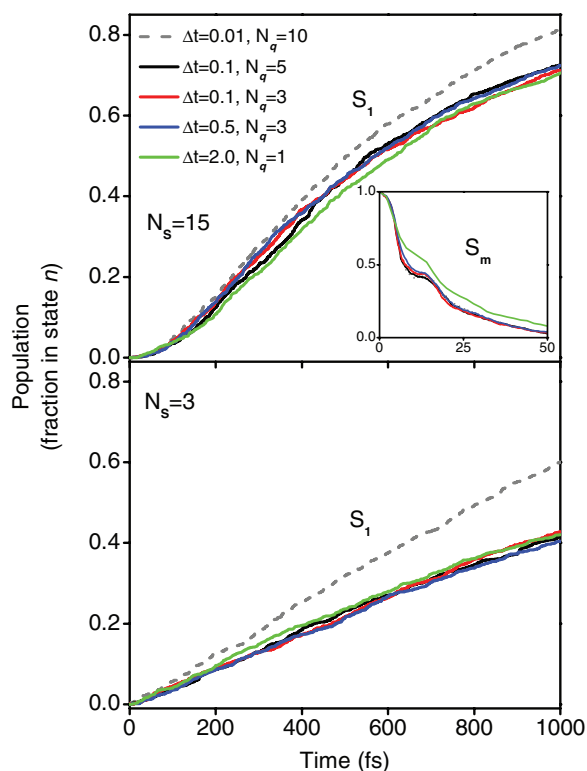


FIG. 2. Comparison of time constants for the  $S_1$  population growth for various combinations of classical integration time steps,  $\Delta t$ , and number of quantum steps,  $N_q$ , for the 1 ps NA-ESMD simulations using 1080 trajectories. (Top) Simulated  $S_m$  relaxation includes  $N_S = 15$  excited states. The inset shows the decay in the initial state ( $S_m$ ) population. (Bottom) Small scale simulation of  $S_2$  relaxation using  $N_S = 3$  excited states

population is shown in the inset, and it consistently occurs within a few tens of femtoseconds. The tested parameters provide good agreement with the accurate simulation and, as expected, the greatest deviation is observed for the  $\Delta t = 2.0$  fs and  $N_q = 1$  simulation. Relaxation time constants were obtained by fitting the rise of the  $S_1$  population curves in Fig. 2 using Eq. (5). The time constants for each set of parameters are listed in Table II along with the percent difference from the reference result. Here, the accurate case (dashed line) yields the fastest relaxation dynamics with a time constant of  $\tau^1 = 404$  fs while recovery of the  $S_1$  population is slower for the other cases. A comparison between the accurate simulation and the other tested parameters reveals that the percent difference in the fitted time constants is consistently in the range of 11 to 15% with the exception of the  $\Delta t = 2.0$  fs and  $N_q = 1$  simulation where a 19% difference is observed. Overall, there is a little difference in the  $S_1$  population growth for the different tested parameters indicating a regime of robust performance.

Next, a series of small-scale simulations was performed monitoring the nonadiabatic relaxation following excitation to state  $S_2$  and a total of  $N_S = 3$  excited states were calculated. The results of these simulations are shown in the bottom panel of Figure 2 for each of the tested parameters using 1080 trajectories, and the fitted relaxation time constants for the rise of the  $S_1$  population and the relative differences are provided in Table II. Again, we observe that the accurate case (dashed line) produced the fastest relaxation dynamics with a time constant of  $\tau^1 = 634$  fs. For the other parameters, recovery of the  $S_1$  population is consistently slower with little dependence on the chosen integration time steps.

Although the changes to the integration time steps produce little variation in the dynamics of the system, there is a large effect on the computational efficiency. As shown in Table I, the associated numerical expense for the “reference” calculation is at least an order of magnitude larger than that associated with the other parameters. Therefore, the computational efficiency can be increased without sacrificing the accuracy of the modeled dynamics. The parameters  $\Delta t = 0.1$  and  $N_q = 3$  have been selected as the standard simulation parameters in order to be consistent with our previous work.<sup>39</sup>

## 2. NACT interpolation

A representative trajectory has been selected from the swarm of trajectories, and the calculated nonadiabatic coupling term coinciding to the first transition,  $S_9 \rightarrow S_8$ , is plotted in Fig. 3. The number of quantum steps,  $N_q$ , was varied while the classical time step was held constant at  $\Delta t = 0.1$  fs. During a typical simulation, the nonadiabatic coupling undergoes rapid fluctuations as a state crossing or region of strong coupling is approached; the NACTs are usually strongly localized peaks. If the chosen value of  $N_q$  is not sufficiently large, then the linear interpolation scheme will cause the nonadiabatic coupling (and transition probability) to be underestimated. In this example, the maximum calculated coupling for  $N_q = 3$  (red circles) is 15% less than the

TABLE II. Relaxation time constants for the  $S_1$  population rise ( $\tau^1$ ) and decay of  $S_m$  population ( $\tau^m$ ) during 1 ps NA-ESMD simulations for 1080 trajectories using various classical and quantum time steps.

Parameters	$\tau_{N_S=15}^1$ (fs)	% difference <sup>a</sup>	$\tau_{N_S=3}^1$ (fs)	% difference	$\tau_{N_S=15}^m$ (fs)	% difference
$\Delta t = 0.01, N_q = 10$	403.6	—	634.1	—	14.9	—
$\Delta t = 0.1, N_q = 5$	460.9	14.2	913.2	44.0	14.6	2.0
$\Delta t = 0.1, N_q = 3$	470.1	16.5	904.1	42.6	14.7	1.3
$\Delta t = 0.5, N_q = 3$	459.3	13.8	940.1	48.3	15.5	4.0
$\Delta t = 2.0, N_q = 1$	489.9	21.4	876.6	38.2	19.3	29.5

<sup>a</sup>% difference with respect to accurate case  $\Delta t = 0.01, N_q = 10$ .

maximum value computed using  $N_q = 5$  (black squares). By analyzing widths of NACT peaks (Fig. 3) occurring due to state crossings along the randomly selected trajectories, we found several very sharp peaks, appearing in cases when the force fields on the states that cross are very different. Consequently, finer time-steps may be necessary to capture such nonadiabatic transitions.

As an example, we point to the decay of the initial  $S_m$  population discussed briefly in Sec. III B 1. The average nonadiabatic coupling for the swarm of 1080 trajectories is shown in the top panel of Fig. 4 for each of the tested set of parameters  $\Delta t$  and  $N_q$ . If the coupling term is substantially underestimated, the system can pass through a region of strong coupling with very low hopping probability causing an otherwise probable transition to be ignored. These large differences in the average NACTs are reflected in the rapid decay of the initial  $S_m$  population shown in the inset of Fig. 2 and in the bottom panel of Fig. 4. To roughly quantify the decay rates, a single exponential fit  $f(t) = \exp(-t/\tau^m)$  has been applied. The resulting time constants and relative deviations are summarized in Table II. The results indicate that the decay of the initial  $S_m$  state is determined by the size of the quantum time step  $\delta t$  (where  $\delta t = \Delta t/N_q$ ). Larger values of  $\delta t$  produce the slowest  $S_m$  decay because they provide lower resolution of the nonadiabatic coupling peaks and underestimate

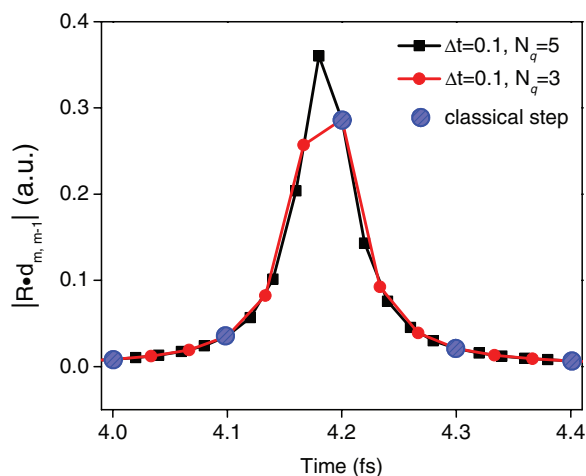


FIG. 3. Calculated NACTs for the first nonadiabatic transition,  $S_m \rightarrow S_{m-1}$  plotted for a single representative trajectory where the number of quantum steps,  $N_q$ , has been varied while the classical time step is held constant at  $\Delta t = 0.1$  fs. For smaller  $N_q = 3$  (red circles), linear interpolation causes the nonadiabatic coupling to be underestimated compared to the larger  $N_q = 5$  calculation (black squares).

transition probabilities. Again, a compromise is required: the selected value of  $N_q$  must be large enough to provide an adequate resolution of the nonadiabatic coupling peaks while maintaining the computational efficiency of the simulation.

### 3. Statistical averaging

The MDQT procedure requires calculation of a large number of trajectories until a statistical convergence is achieved. For middle size to large polyatomic molecules, propagating a large swarm of trajectories can be prohibitively expensive. This commonly leads to improper evaluation of the minimum number of trajectories required to achieve the desired accuracy. Therefore, in order to investigate how the

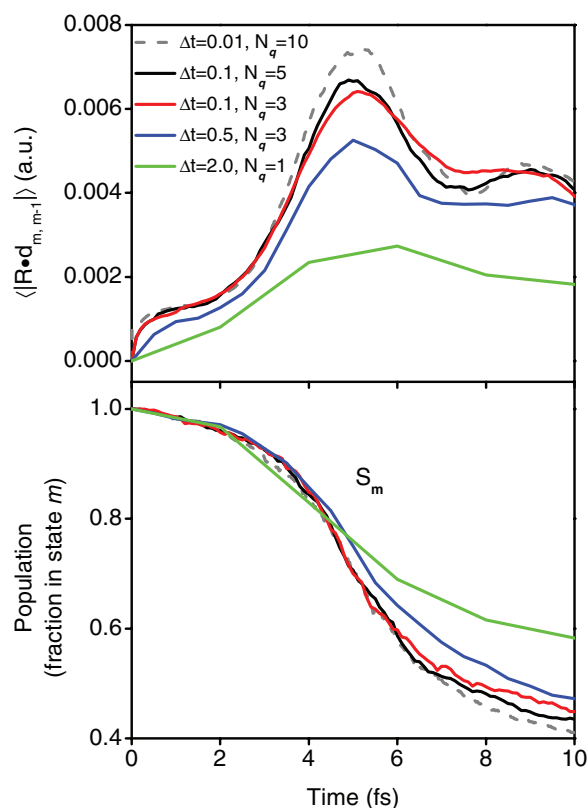


FIG. 4. (Top) NACTs averaged over the swarm of 1080 trajectories are shown for the various combinations of classical integration time steps,  $\Delta t$ , and a number of quantum steps,  $N_q$ . During the first few fs of the NA-ESMD simulation all trajectories still remain in the initial  $S_m$  state. (Bottom) The decay rate of the initial  $S_m$  state population at early times corresponds to the computed value of the nonadiabatic coupling.

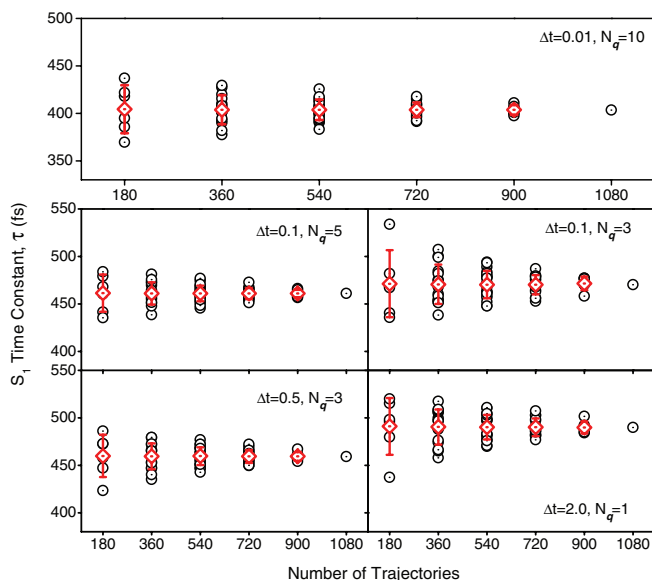


FIG. 5. Calculated time constants for the  $S_1$  population growth. Here the number of independent trajectories included in the average has been varied, and all possible combinations of batches are shown ( $\odot$ ). Each combination of classical time step,  $\Delta t$ , and number of quantum steps,  $N_q$ , is shown in a separate panel along with the accurate reference calculation  $\Delta t = 0.01$  fs and  $N_q = 10$ . The average time constant is also indicated ( $\diamond$ ) and the error bars represent the standard deviation.

convergence depends on the number of independent trajectories included in the average, we divide the simulation into 6 batches (each batch containing 180 trajectories) and consider how the results are affected by the addition of each new batch. All possible unique combinations of batches are considered, and our analysis include: 180 trajectories (6 combinations of 1 batch), 360 trajectories (15 combinations of 2 batches), 540 trajectories (20 combinations of 3 batches), 720 trajectories (15 combinations of 4 batches), 900 trajectories (6 combinations of 5 batches), and 1080 trajectories (1 combination of 6 batches).

The time constant  $\tau$  for the rise of the  $S_1$  population was determined for each combination by fitting the associated curve to Eq. (5). Analysis of the variance (standard deviation) from the average time constant at different numbers of trajectories provides insight into the convergence behavior. The time constants for each of the combinations, the average time constant, and the variance for each set of tested parameters  $\Delta t$  and  $N_q$  are plotted in Fig. 5, and the data is provided in Table III. The calculated time constants for the  $S_1$  population

growth are plotted for all possible combinations of batches together with the average time constant and the error bars representing the variance. For a given set of parameters, we observe only a slight fluctuation in the average time constant as the number of trajectories is increased. We have attributed this noise to be a by-product of the error associated with the fit; we expect that fitting multiple batches and then averaging their time constants should produce (nearly) the same result as averaging the multiple batches first and then fitting the data.

Our analysis indicates that for all tested parameters, for the given molecule, a minimum of 360 trajectories must be computed in order to reach a converged result with less than 5% standard deviation. This can be further reduced to 2% if 720 trajectories are included. Generally, we observe that the improvement in accuracy associated with each additional batch diminishes so that the benefit from computing extra trajectories is no longer worth the additional numerical cost.

#### 4. Random seed

Each trajectory is assigned a random seed to initialize the random number generator which is used for both the stochastic force in Langevin dynamics and for accepting or rejecting state transitions in the surface hopping algorithm. In all simulations, a different random seed is used for each independent trajectory in order to avoid trajectory “synchronization.”<sup>51</sup> To illustrate the effect of random seed change, the 1 ps NA-ESMD simulation was repeated for 1080 trajectories using both the standard time steps ( $\Delta t = 0.1$  fs,  $N_q = 3$ ) and the accurate “reference” time steps ( $\Delta t = 0.01$  fs,  $N_q = 10$ ). The random seed assigned to each of the 1080 trajectories was changed compared to the reference simulation while all other parameters and initial geometries were preserved. The results are presented in Fig. 6 where the population build-up curves are shown. As expected, the decay of the  $S_m$  population is not affected by the change in seed since the associated time scale is relatively short. However, the alternate seed assignments do cause variation of the  $S_1$  population for both simulations. In both cases, the alternate seed choice lead to about 10% increase in the computed relaxation time constants  $\tau^1$ , where the calculated time constants are 470 fs and 404 fs for the original standard and accurate simulations, respectively. The simulation with the alternate seed produced fitted time constants of 420 fs and 365 fs for the standard and accurate simulations, respectively. This  $\sim 10\%$  variation of the

TABLE III. Average relaxation time constants ( $\tau_{avg}^1 \pm \tau_{std}^1$ , fs) for the  $S_1$  population rise computed for 1 ps NA-ESMD simulations with various numbers of independent trajectories.

Number of trajectories	$\Delta t = 0.01$ $N_q = 10$	$\Delta t = 0.1$ $N_q = 5$	$\Delta t = 0.1$ $N_q = 3$	$\Delta t = 0.5$ $N_q = 3$	$\Delta t = 2.0$ $N_q = 1$
180	404.5 $\pm$ 25.3	461.4 $\pm$ 19.6	471.3 $\pm$ 35.4	459.9 $\pm$ 22.4	491.0 $\pm$ 30.0
360	403.9 $\pm$ 15.2	461.1 $\pm$ 11.7	470.6 $\pm$ 20.7	459.5 $\pm$ 13.5	490.4 $\pm$ 18.5
540	403.7 $\pm$ 10.7	461.0 $\pm$ 8.24	470.3 $\pm$ 14.4	459.7 $\pm$ 9.4	490.2 $\pm$ 13.1
720	403.7 $\pm$ 7.6	461.0 $\pm$ 5.9	470.2 $\pm$ 10.3	459.3 $\pm$ 6.8	490.1 $\pm$ 9.4
900	403.6 $\pm$ 5.1	461.0 $\pm$ 3.9	471.6 $\pm$ 7.2	459.3 $\pm$ 4.6	490.0 $\pm$ 6.3
1080	403.6	460.9	470.1	459.3	489.9

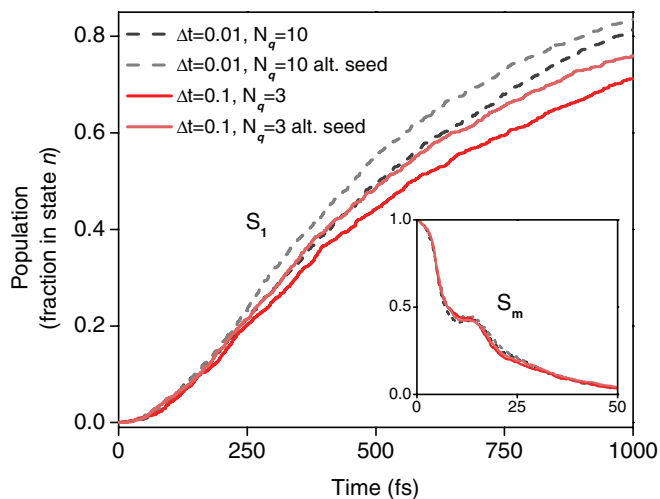


FIG. 6.  $S_1$  population growth during 1 ps NA-ESMD simulations where the random seed has been varied. Comparison of the accurate simulation ( $\Delta t = 0.01$  fs and  $N_q = 10$ ) and the standard simulation ( $\Delta t = 0.1$  fs and  $N_q = 3$ ) are shown. The decay of the initial state ( $S_m$ ) population is shown in the inset. The generated random number series affects both the stochastic force and the surface hopping algorithm.

calculated rates represents a statistical fluctuation due to lack of complete statistical averaging.

## C. MDQT approximations

### 1. NACT simplification schemes

A common approximation used to mitigate the computational bottleneck imposed by the evaluation of NACTs is to reduce the number of coupling terms included in the simulation. These approximations, however, not only restrict the classical hopping between states but also impact the evolution of the quantum coefficients and prevent quantum population transfer between states which can have a less predictable effect on dynamics. We have tested the validity of these approximations by comparing the partial coupling (PC) and two-state (TS) schemes to the complete coupling (CC) picture. Table IV contains the number of coupling terms ( $N_C$ ) computed for each model as well as the computed relaxation time constants.

We first analyze a simple case where  $N_S = 3$  excited states have been computed and the initial state  $S_2$  has been populated. Such few-state models have been extensively used in previous studies for testing various surface hopping schemes.<sup>73–75</sup> Here our standard NA-ESMD simulation parameters have been employed using 180 trajectories. The re-

TABLE IV. Number of computed NACTs ( $N_C$ ) and computed relaxation time constants ( $\tau^1$ ) for 1 ps NA-ESMD simulations using various NACT approximate schemes.

Model	$N_C$	$\tau_{N_S=15}^1$ (fs)	$\tau_{N_S=3}^1$ (ps)
complete coupling (CC)	$1/2 N_S(N_S - 1)$	470.1	1.19
partial coupling (PC)	$N_S - 1$	937.6	1.39
two-state (TS)	1	3420 <sup>a</sup>	1.46

<sup>a</sup>Corresponds to the  $S_2$  population rise,  $S_1$  is not populated during TS simulation with  $N_S = 15$ .

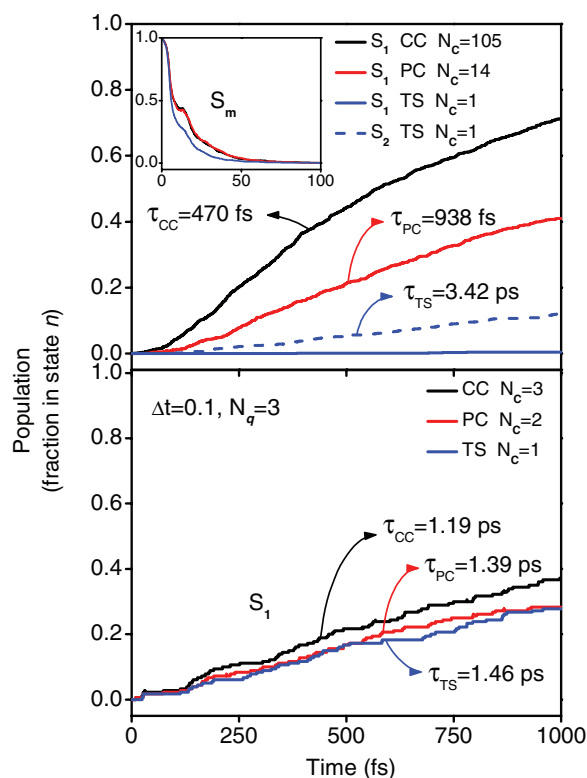


FIG. 7. Approximate NACT cutting schemes (PC and TS) are compared to the CC simulation. (Top) The  $S_1$  population rise during the standard 1 ps NA-ESMD simulations with 1080 trajectories using  $N_S = 15$  excited states (solid lines). The  $S_2$  population rise for the TS simulation is also shown (dashed line). The inset shows the decay of the initial state ( $S_m$ ) population. (Bottom) Same as the top, but using  $N_S = 3$  excited states and 180 trajectories with  $S_2$  being the initial excited state.

sults for this simple test case are shown in the bottom panel of Fig. 7, where the time constants for the  $S_1$  population rise are 1.19 ps, 1.39 ps, and 1.46 ps for the CC, PC, and TS models, respectively. The results for our three-state dynamics are in a good agreement to a similar comparison done by Pittner *et al.*<sup>52</sup> for the three-state simulation of methaniminium cation with  $S_2$  being initially populated. This work has shown that both TS and PC approximations produce acceptable results and reproduce the essential features observed in the CC modeling. Indeed, for such small scale simulations involving only a few excited states, the approximate NACT schemes are valid and work quite well with no significant impact on the observed dynamics.

However, the automatic extrapolation of these approximations to multi-state simulations can be misleading. It has not yet been investigated whether these approximations can be successfully applied to modeling involving larger numbers of excited states. The number of coupling terms that are omitted from the approximate models increases quadratically with the number of excited states used (Table IV). The comparison of the CC, PC, and TS models for the standard 1 ps NA-ESMD simulation of  $mA_g$  relaxation dynamics using  $N_S = 15$  excited states is shown in the top panel of Fig. 7. Here TS, PC, and CC models produce vastly different results. In fact, for the two-state model  $S_1$  is not populated over the entire course of 1 ps dynamics and even  $S_2$  (dashed line) has over a seven-fold increase in relaxation time constant compared to the complete



coupling model. The partial coupling model fails to reproduce the CC results as well, indicating that it is not only the electronic couplings of the current state that are important, but the nonadiabatic couplings between all pairs of states are needed in order to capture the true dynamics.

## 2. Classical-path approximation

The validity of the CPA has been tested by performing the standard 1 ps NA-ESMD simulation of the  $S_m$  state relaxation in distyrylbenzene using the nuclear evolution from a single ground electronic state trajectory as an input for all excited state trajectories during nonadiabatic dynamics. The results invoking the CPA and our reference data are compared in Fig. 8. The time constants  $\tau_{CPA}^1$  and  $\tau_{ref}^1$  corresponding to the calculations with and without the CPA implementation, have values of 622 fs and 470 fs, respectively. While the relaxation rate is slowing down by about 30% in the CPA, Figure 8 clearly shows that the relaxation dynamics is different for the two simulations. The most striking result of this comparison is the slow decay of the initial  $S_m$  population with respect to the reference simulations. In consequence, the  $S_1$  population growth rate substantially decreases in the CPA calculation. This fact can be attributed to differences in the conformational space followed by both type of simulations due to different force fields being used. Utilization of the “native” excited state gradients promotes vibrational relaxation toward the excited state optimal geometry, thus facilitating more frequent surface crossings. Moreover, according to Eq. (4), the value of the NACT terms can be strongly affected by the effective nuclear velocities in the direction of the nonadiabatic coupling vector. This feature cannot be adequately addressed in the CPA representation.

## D. Friction coefficient for Langevin dynamics

In order to analyze the dissipation effects on the NA-ESMD simulations, the friction coefficient  $\gamma$  has been varied

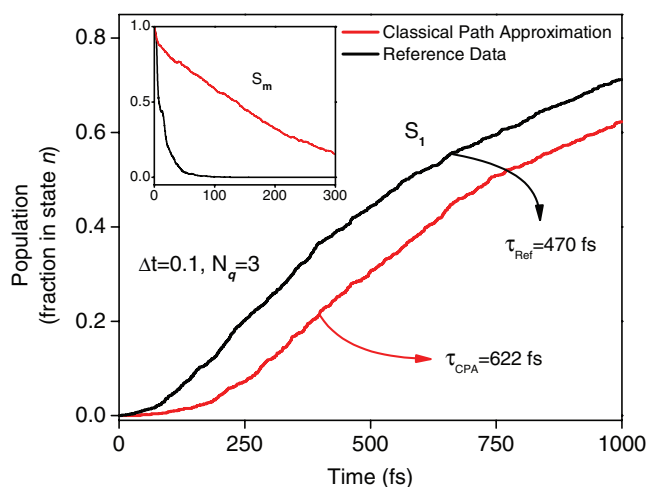


FIG. 8.  $S_1$  population growth during 1 ps NA-ESMD simulation using the classical-path approximation compared to the reference calculation which uses the actual excited state energy gradients. The inset shows the decay in the initial state ( $S_m$ ) population.

TABLE V. Relaxation time constant ( $\tau^1$ ) and average temperature calculated for various friction coefficients  $\gamma$  for the standard 1 ps NA-ESMD simulations.

$\gamma$ ( $\text{ps}^{-1}$ )	$\tau^1$ (fs)	$T_{avg}$ (K)	$T_{rms}^a$ (K)
0.2	357.9	324	30
2.0	470.1	302	3.8
20	541.7	300	1.4

<sup>a</sup>The reference temperature is  $T_0 = 300$  K.

by two orders of magnitude from  $0.2 \text{ ps}^{-1}$  to  $20 \text{ ps}^{-1}$ . Results are summarized in Table V where the computed time constants  $\tau^1$ , as well as the average temperature and its corresponding deviations during the dynamics are shown. The top panel in Fig. 9 displays the calculated  $S_m$  state relaxation in distyrylbenzene using different  $\gamma$  values. Overall, observed vibronic relaxation (the decay of the initial state  $S_m$  and the accompanying rise of  $S_1$  population) is slowing with increasing  $\gamma$  values. Larger viscosity overdamps nuclear relaxation. For example, low  $\gamma$  values reveal recurrence in the population of the  $S_m$  state (see inset in Fig. 9), which disappears as  $\gamma$  increases due to dephasing and solvent friction. Consequently, the conformational space is sampled at a slower pace for large  $\gamma$  values, thus reducing the effective rate of state crossings. Moreover, the faster vibrational damping, particularly in the direction of the nonadiabatic coupling vector, has

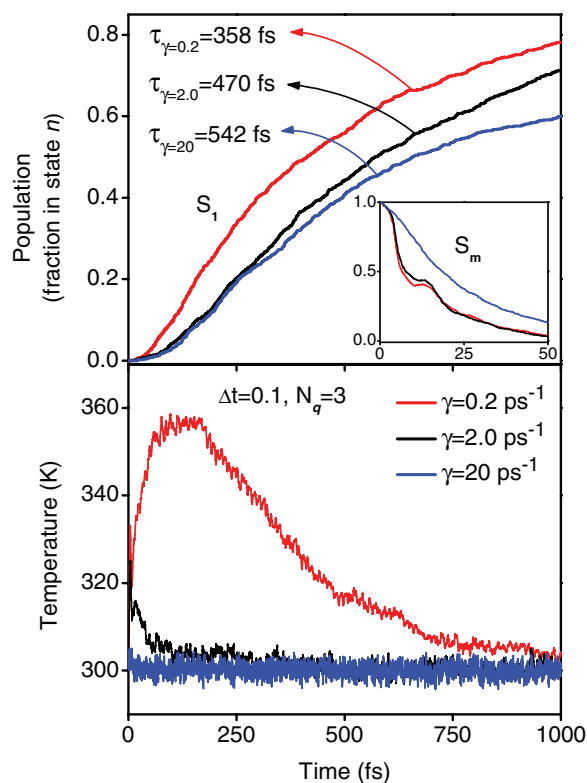


FIG. 9. Comparison of 1 ps NA-ESMD simulations with 1080 trajectories using friction coefficient values  $\gamma = 0.2, 2.0,$  and  $20 \text{ ps}^{-1}$  and a Langevin thermostat temperature  $T_0 = 300$  K. (Top) The  $S_1$  population rise. The inset shows the decay in the initial state ( $S_m$ ) population. (Bottom) The time-dependence of temperature averaged over an ensemble of trajectories. The larger  $\gamma$  produces high temperature fidelity while a smaller  $\gamma$  causes large temperature fluctuations.

the concomitant effect of reducing the values of the nonadiabatic coupling terms (see Eq. (4)). All these factors lead to an increase of the excited state lifetimes (compare the population rise for the  $S_1$  state for different  $\gamma$  values in Fig. 9). The respective time dependence of the average temperature is shown in the bottom panel in Fig. 9.  $\gamma$  can be thought of as the coupling between the system and the bath, which transfers vibrational energy to the solvent. As can be seen, larger  $\gamma$  values lead to a faster transfer of the excess energy to the solvent, while significant vibrational heating is observed for the smallest  $\gamma = 0.2 \text{ ps}^{-1}$  due to energy transfer from electronic to vibrational degrees of freedom of the molecule.

The friction coefficient also impacts the rate of conformational sampling. We next analyze how the chosen friction coefficient influences the required length of the initial GS trajectory for MDQT. Three ground-state trajectories of 6 ns in length were computed using different friction coefficients of  $0.2 \text{ ps}^{-1}$ ,  $2.0 \text{ ps}^{-1}$ , and  $20 \text{ ps}^{-1}$  for each trajectory. After the molecule had been equilibrated in the ground-state for 1 ns, the geometries were sampled at 1 ps intervals for 10 ps, 100 ps, 500 ps, 1 ns, or 5 ns (reference simulation) to simulate trajectories of varying length. In order to determine the degree of conformational sampling within the system we monitor the torsion angle  $\theta$  corresponding to the rotation around

the double-bond of the vinylene segment, corresponding to a “soft” librational motion characteristic for such molecules. Histograms of the sampled angles are shown in Fig. 10. These histograms have been normalized to facilitate comparison and the same y-axis and x-axis scales are used in each panel. The insets provide a rescaled view of the tail of the histograms. We expect that upon  $t \rightarrow \infty$  obtained distributions should be independent of  $\gamma$ . Indeed, our reference 5 ns spectra are very similar for all  $\gamma$  values used.

At the 10 ps level, obtained sampling is poor and does not represent the true conformational space. The 100 ps trajectory offers substantial improvement while at the 500 ps level, most of the critical features of the 5 ns spectrum are reproduced. The insets in Fig. 10 reveal that the degree of sampling for larger angles is affected by the friction coefficient. For  $\gamma = 0.2 \text{ ps}^{-1}$  angles up to  $\theta = 20^\circ$  are well sampled at the 100 ps level. In fact, large angles are oversampled in comparison to the reference spectrum. For  $\gamma = 2.0 \text{ ps}^{-1}$  the same angles are sampled to a lesser extent and there is less oversampling with respect to the reference spectrum. However, for  $\gamma = 20 \text{ ps}^{-1}$  the 100 ps spectrum *undersamples* the large angles with respect to the 5 ns spectrum and has sufficiently less sampling compared to the  $0.2 \text{ ps}^{-1}$  and  $2.0 \text{ ps}^{-1}$  spectra. In general, the ground state trajectory should be lengthened for larger  $\gamma$  values to obtain complete conformational sampling for a given molecular system.

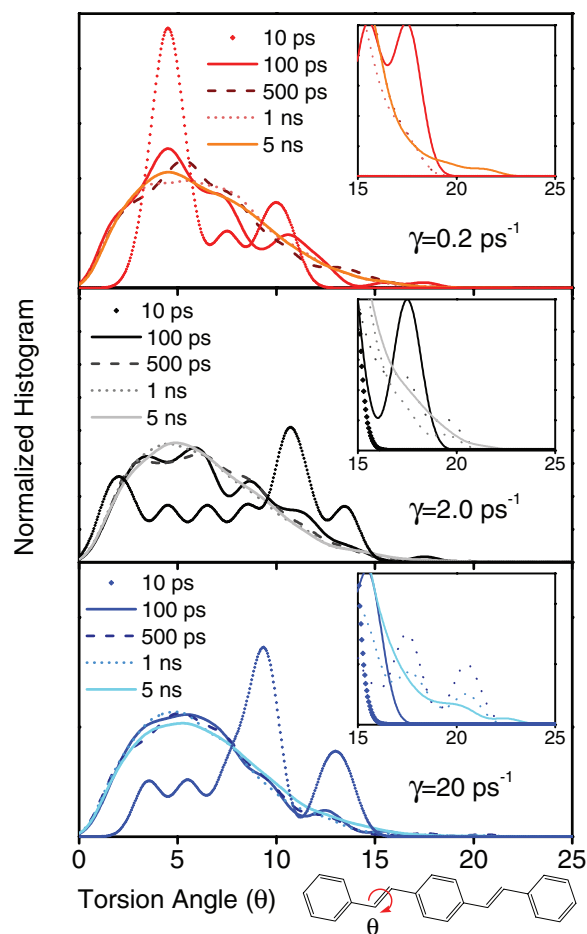


FIG. 10. The histogram of the torsion angles  $\theta$  sampled over the ground state trajectory for different friction coefficients. Here 1 ns equilibration time is used followed by a sampling period of 10 ps, 100 ps, 500 ps, 1 ns, and 5 ns from which the initial geometries and velocities are taken at 1 ps intervals.

#### IV. CONCLUSIONS

Numerical simulations beyond Born-Oppenheimer approximation are very expensive. Consequently, for past decades numerous algorithms developed for nonadiabatic dynamics simulations have been tested primarily on only model systems such as numerically tabulated potential energy surfaces of a few excited states for several vibrational coordinates. Advances of quantum chemistry, numerical algorithms and computer technology currently make it possible to apply previously developed machinery for nonadiabatic dynamics simulations to realistic molecular systems. Such modeling is challenging partially due to the fact that previously developed and commonly used simplifications that generally work well in the model case, may fail for realistic molecules with tens of excited states, hundreds of vibrational degrees of freedom and strongly varying vibrational frequencies and electron-phonon coupling constants. Our NA-ESMD simulations presented here clarify some of these issues.

One of the simplest and most effective ways to reduce numerical cost of NAMD simulations is to increase the classical and quantum integration time steps. In doing so, however, one must take caution to ensure that the selected parameters are within an acceptable range of accuracy and do not produce any deleterious effects on the simulated dynamics. The net hopping probabilities calculated from the FSSH algorithm for a finite time are ideally independent of the integration time step. When the system is in a region of strong coupling, however, time step independence may not be maintained since the value of the nonadiabatic coupling changes rapidly. In these regions, where a state switch is likely to occur, the dynamics may depend on the chosen integration time step, which

should correctly resolve the nonadiabatic coupling peaks. The balance between selecting an appropriate classical and quantum time step (sufficient to resolve the nonadiabatic coupling peaks) while maintaining a manageable cost, requires close attention.

One can also imagine an algorithm in which the quantum time step can be adjusted on the fly by monitoring the values of  $d(\text{NACT})/dt$  and/or  $d(\text{NACT})/dR$  to detect when the system is approaching a coupling region and then reducing the quantum time step by some specified factor until the peak is resolved. However, care must still be taken in selecting the appropriate parameters used to detect coupling regions. Regardless of the approach, the optimal parameters may differ from system to system. It is therefore convenient to start by running a few trial trajectories using different  $\Delta t$  and  $N_q$  parameters. The results should provide necessary information on the width of NACT peaks, which may be very narrow when the force fields on the states that cross are substantially different. Using this approach, the resolution of the nonadiabatic coupling terms can be verified before running a swarm of trajectories for a large-scale simulation. Using our NA-ESMD package we have shown that, for future simulations, it is possible to use larger classical time steps while retaining reasonable accuracy.

As expected, the assignment of the random seed used for the stochastic surface hopping algorithm and Langevin dynamics has only a small effect on the computed dynamics and results in less than 10% statistical fluctuations in the calculated rates. Consequently, any random seed effects will be washed out after averaging over a sufficiently large number of trajectories. Although about 400 trajectories is found to be sufficient to achieve reasonable statistical convergence of the calculated time constants, a larger number is desirable to attain better accuracy and to eliminate random seed effects. In order to eliminate the statistical fluctuations caused by the random seed assignments, one would have to average not only over an ensemble of geometries but over a range of random seeds as well. In other words, multiple trajectories would need to be computed for the same geometry starting from different random seeds. However, we find that the dependence on the random seed is not large enough to justify extra computational effort that would be required to compute additional trajectories. We consider 400 trajectories to be a reliable minimum standard for the NA-ESMD simulations. Generally, the number of trajectories required to reach the converged result may depend on the amount of conformational variation in the molecular system under investigation.

Approximations for MDQT simulations should be applied only after careful consideration. NACT cutting schemes, which reduce the computational cost associated with the coupling term by evaluating only a portion of the NACTs, offer increased savings for simulations involving more and more excited states. However, we have shown that these approximations are only valid for simulations involving only a few (2–3) excited states. The transition probability that changes classical populations depends on the relative change of the quantum coefficients. These changes are expressed as a sum of contributions of couplings with all other states and are proportional to the NACTs (see Eq. (2)). A reduction in the

number of NACT terms leads to a truncation of this summation and reduces the change in the populations as well as the hops. Some fraction of the quantum population must be transferred to the new state before a state switch can occur. In the truncated models, all pathways for population transfer that do not involve the current state are eliminated. As fewer coupling terms are included, the pathways to build the quantum population of the new states become more restricted and the calculated relaxation becomes slower. In addition to restricting the population transfer, the TS model confines the system to a sequential state-by-state relaxation and eliminates decay pathways in which the system hops over multiple states. Even though the partial coupling and two-state simplifications may seem to be very attractive in cases involving many excited states, this is exactly when they should be avoided.

Another approximation, the Classical-Path Approximation, resulted in a significant change to the simulated relaxation dynamics. This indicates that the forces generated by the photoexcited electronic subsystem should be properly included in the nuclear evolution when modeling molecular systems with substantial electron-phonon coupling constants.

By virtue of the fluctuation-dissipation theorem derived by Langevin, the friction coefficient must be proportional to the stochastic force variance, which controls the temperature fluctuations.<sup>76</sup> As expected, a friction coefficient of  $2.0 \text{ ps}^{-1}$  provides balanced temperature coupling without the dampening effect on the dynamics associated with larger values. Our results are in good agreement with the findings of Paterlini and Ferguson<sup>63</sup> which demonstrated that  $\gamma$  in the range of 1 to  $5 \text{ ps}^{-1}$  is an optimum parameter for Langevin dynamics simulations in water. Overall we observe that larger  $\gamma$  values result in slower vibrational relaxation of photoexcited states. Moreover, for larger  $\gamma$  values, the ground-state trajectory from which initial geometries and velocities are sampled for subsequent nonadiabatic dynamics modeling must be lengthened to obtain adequate conformational sampling. In general, we find that a 500 ps ground-state trajectory at the room temperature is sufficient to capture the same degree of sampling as longer 1 ns and 5 ns trajectories.

The proper choice of the friction coefficient would then clearly affect the time scale of the process, but at least in the cases presented here, it does not affect the physical picture behind the intraband relaxation. The actual choice of the friction coefficient value is a subject of interest. For example, the value based on experimental viscosity may be different than the value computed from explicit solvent simulations with current force fields. Little or no work has been done for solvents other than water. In the future, as we move towards explicit solvent simulations, the choice of the friction coefficient value will no longer be a concern.

In summary, we have demonstrated that user-defined parameters and approximations for nonadiabatic excited state molecular dynamics simulations have substantial impact on the quality of calculated results. It is essential to give proper consideration to each system under investigation when choosing parameters such as integration time steps and the number of independent trajectories to be computed for the stochastic surface hopping algorithms.

## ACKNOWLEDGMENTS

T.N. and S.T. acknowledge support of the (U.S.) Department of Energy and Los Alamos National Laboratory (LANL) Directed Research and Development funds. This work was partially supported by CONICET, AMPCGT Grant No. PICT-2010-2375, UNQ, NSF Grants CHE-0239120 and CHE-0808910. LANL is operated by Los Alamos National Security, LLC, for the National Nuclear Security Administration of the (U.S.) Department of Energy under contract DE-AC52-06NA25396. We acknowledge support of Center for Integrated Nanotechnology (CINT) and Center for Nonlinear Studies (CNLS) at LANL.

- <sup>1</sup>M. Ben-Num, J. Quenneville, and T. J. Martinez, *J. Phys. Chem. A* **104**, 5161 (2000).
- <sup>2</sup>M. J. Bedard-Hearn, F. Sterpone, and P. J. Rossky, *J. Phys. Chem. A* **114**, 7661 (2010).
- <sup>3</sup>M. J. Bearpark, F. Bernardi, S. Clifford, M. Olivucci, M. A. Robb, B. R. Smith, and T. Vreven, *J. Am. Chem. Soc.* **118**, 169 (1996).
- <sup>4</sup>G. Granucci and M. Persico, *Theor. Chem. Acc.* **117**, 1131 (2007).
- <sup>5</sup>G. Granucci, M. Persico, and A. Toniolo, *J. Chem. Phys.* **114**, 10608 (2001).
- <sup>6</sup>C. F. Craig, W. R. Duncan, and O. V. Prezhdo, *Phys. Rev. Lett.* **95**, 163001 (2005).
- <sup>7</sup>O. V. Prezhdo, W. R. Duncan, and V. V. Prezhdo, *Prog. Sur. Sci.* **84**, 30 (2009).
- <sup>8</sup>S. Fernandez-Alberti, V. D. Kleiman, S. Tretiak, and A. E. Roitberg, *J. Phys. Chem. Lett.* **1**, 2699 (2010).
- <sup>9</sup>P. R. L. Markwick and N. L. Doltsinis, *J. Chem. Phys.* **126**, 175102 (2007).
- <sup>10</sup>I. Antol, M. Eckert-Maksic, M. Barbatti, and H. Lischka, *J. Chem. Phys.* **127**, 234303 (2007).
- <sup>11</sup>G. Zechmann, M. Barbatti, H. Lischka, J. Pittner, and V. Bonacic-Koutecky, *Phys. Chem. Lett.* **418**, 377 (2006).
- <sup>12</sup>M. Barbatti, G. Granucci, M. Persico, and H. Lischka, *Phys. Chem. Lett.* **401**, 276 (2005).
- <sup>13</sup>B. R. Smith, M. J. Bearpark, M. A. Robb, F. Bernardi, and M. Olivucci, *Phys. Chem. Lett.* **242**, 27 (1995).
- <sup>14</sup>S. Ramakrishna, F. Willig, V. May, and A. Knorr, *J. Phys. Chem. B* **107**, 607 (2003).
- <sup>15</sup>A. H. Zewail, *J. Phys. Chem. A* **104**, 5660 (2000).
- <sup>16</sup>J. Tully, *J. Chem. Phys.* **93**, 1061 (1990).
- <sup>17</sup>X. Li, J. Tully, H. Schlegel, and M. Frisch, *J. Chem. Phys.* **123**, 84106 (2005).
- <sup>18</sup>P. V. Parandekar and J. C. Tully, *J. Chem. Theory Comput.* **2**, 229 (2006).
- <sup>19</sup>J.-Y. Fang and S. Hammes-Schiffer, *J. Chem. Phys.* **110**, 11166 (1999).
- <sup>20</sup>K. Drukker, *J. Comput. Phys.* **153**, 225 (1999).
- <sup>21</sup>S. Hammes-Schiffer and J. C. Tully, *J. Chem. Phys.* **101**, 4657 (1994).
- <sup>22</sup>P. V. Parandekar and J. C. Tully, *J. Chem. Phys.* **122**, 094102 (2005).
- <sup>23</sup>J.-Y. Fang and S. Hammes-Schiffer, *J. Chem. Phys.* **106**, 8442 (1997).
- <sup>24</sup>U. Müller and G. Stock, *J. Chem. Phys.* **107**, 6230 (1997).
- <sup>25</sup>J. E. Subotnik and N. Shenvi, *J. Chem. Phys.* **134**, 024105 (2011).
- <sup>26</sup>M. D. Hack, A. W. Jasper, Y. L. Volobuev, D. W. Schwenke, and D. G. Truhlar, *J. Phys. Chem. A* **103**, 6309 (1999).
- <sup>27</sup>T. Takayanagi, Y. Kurosaki, and A. Ichihara, *J. Chem. Phys.* **112**, 2615 (2000).
- <sup>28</sup>S. Chapman, *Adv. Chem. Phys.* **82**, 423 (1992).
- <sup>29</sup>S. Fernandez-Alberti, N. Halberstadt, J. A. Beswick, and J. Echave, *J. Chem. Phys.* **109**, 2844 (1998).
- <sup>30</sup>I. H. Gersonde and H. Gabriel, *J. Chem. Phys.* **98**, 2094 (1993).
- <sup>31</sup>A. I. Krylov and R. B. Gerber, *J. Chem. Phys.* **106**, 6574 (1997).
- <sup>32</sup>G. Pierdominici-Sottile, S. Fernandez-Alberti, and J. Palma, *Adv. Quantum Chem.* **59**, 247 (2010).
- <sup>33</sup>F. Plasser and H. Lischka, *J. Chem. Phys.* **134**, 034309 (2011).
- <sup>34</sup>S. Y. Kim and S. Hammes-Schiffer, *J. Chem. Phys.* **119**, 4389 (2003).
- <sup>35</sup>M. N. Kobraik and S. Hammes-Schiffer, *J. Phys. Chem. B* **105**, 10435 (2001).
- <sup>36</sup>E. Fabiano, T. W. Keal, and W. Thiel, *Chem. Phys.* **349**, 334 (2008).
- <sup>37</sup>G. A. Worth, M. A. Robb, and B. Lasorne, *Mol. Phys.* **106**, 2077 (2008).
- <sup>38</sup>B. Lasorne, M. A. Robb, and G. A. Worth, *Phys. Chem. Chem. Phys.* **9**, 3210 (2007).
- <sup>39</sup>T. Nelson, S. Fernandez-Alberti, V. Chernyak, A. E. Roitberg, and S. Tretiak, *J. Phys. Chem. B* **115**, 5402 (2011).
- <sup>40</sup>S. Fernandez-Alberti, V. D. Kleiman, S. Tretiak, and A. E. Roitberg, *J. Phys. Chem. A* **113**, 7535 (2009).
- <sup>41</sup>S. Tretiak and S. Mukamel, *Chem. Rev.* **102**, 3171 (2002).
- <sup>42</sup>V. Chernyak, M. F. Schulz, S. Mukamel, S. Tretiak, and E. V. Tsiper, *J. Chem. Phys.* **113**, 36 (2000).
- <sup>43</sup>S. Tretiak, C. Isborn, A. Niklasson, and M. Challacombe, *J. Chem. Phys.* **130**, 054111 (2009).
- <sup>44</sup>F. Furche and R. Ahlrichs, *J. Chem. Phys.* **117**, 7433 (2002).
- <sup>45</sup>S. Tretiak and V. Chernyak, *J. Chem. Phys.* **119**, 8809 (2003).
- <sup>46</sup>M. Tommasini, V. Chernyak, and S. Mukamel, *Int. J. Quantum Chem.* **85**, 225 (2001).
- <sup>47</sup>V. Chernyak and S. Mukamel, *J. Chem. Phys.* **112**, 3572 (2000).
- <sup>48</sup>R. Send and F. Furche, *J. Chem. Phys.* **132**, 044107 (2010).
- <sup>49</sup>S. Tretiak, A. Saxena, R. L. Martin, and A. R. Bishop, *Phys. Rev. Lett.* **89**, 097402 (2002).
- <sup>50</sup>I. Franco and S. Tretiak, *Chem. Phys. Lett.* **372**, 403 (2003).
- <sup>51</sup>D. J. Sindhikara, S. Kim, A. F. Voter, and A. E. Roitberg, *J. Chem. Theory Comput.* **5**, 1624 (2009).
- <sup>52</sup>J. Pittner, H. Lischka, and M. Barbatti, *Chem. Phys.* **356**, 147 (2009).
- <sup>53</sup>M. Barbatti and H. Lischka, *J. Am. Chem. Soc.* **130**, 6831 (2008).
- <sup>54</sup>G. Stock and M. Thoss, *Adv. Chem. Phys.* **131**, 243 (2005).
- <sup>55</sup>H. Hirai and O. Sugino, *Phys. Chem. Chem. Phys.* **11**, 4570 (2009).
- <sup>56</sup>M. Feig, *J. Chem. Theory Comput.* **3**, 1734 (2007).
- <sup>57</sup>B. Zagrovic and V. Pande, *J. Comput. Chem.* **24**, 1432 (2003).
- <sup>58</sup>S. Mukamel, S. Tretiak, T. Wagersreiter, and V. Chernyak, *Science* **277**, 781 (1997).
- <sup>59</sup>S. Tretiak, V. Chernyak, and S. Mukamel, *J. Chem. Phys.* **105**, 8914 (1996).
- <sup>60</sup>S. Tretiak, W. M. Zhang, V. Chernyak, and S. Mukamel, *Proc. Nat. Acad. Sci. U.S.A.* **96**, 13003 (1999).
- <sup>61</sup>M. P. Allen and D. J. Tildesley, *Computer Simulation of Liquids* (Clarendon, Oxford, 1987).
- <sup>62</sup>W. C. Swope, H. C. Andersen, P. H. Berens, and K. R. Wilson, *J. Chem. Phys.* **76**, 637 (1982).
- <sup>63</sup>M. Paterlini and D. Ferguson, *Chem. Phys.* **236**, 243 (1998).
- <sup>64</sup>S. K. Park and K. W. Miller, *Commun. ACM* **31**, 1192 (1988).
- <sup>65</sup>W. H. Press, S. A. Teukolsky, W. T. Vetterling, and B. P. Flannery, *Numerical Recipes in Fortran 77: The Art of Scientific Computing*, 2nd ed. (Cambridge University Press, Cambridge, England, 1996).
- <sup>66</sup>T. E. Hull, W. H. Enright, and K. R. Jackson, "User's guide for DVERK – A subroutine for solving non-stiff ODEs," Technical Report 100, Department of Computer Science, University of Toronto, Canada, 1976.
- <sup>67</sup>IMSL MATH/LIBRARY Special Functions, Visual Numerics, Inc., USA.
- <sup>68</sup>M. P. Allen and D. J. Tildesley, *Computer Simulation of Liquids* (Oxford University Press, New York, 1990).
- <sup>69</sup>M. Chandross and S. Mazumdar, *Phys. Rev. B* **55**, 1497 (1997).
- <sup>70</sup>S. V. Frolov, Z. Bao, M. Wohlgenannt, and Z. V. Vardeny, *Phys. Rev. Lett.* **85**, 2196 (2000).
- <sup>71</sup>I. Baraldi, G. Ginocchietti, U. Mazzucato, and A. Spalletti, *Chem. Phys.* **337**, 168 (2007).
- <sup>72</sup>S. Brazovskii, N. Kirova, and A. R. Bishop, *Opt. Mater.* **9**, 472 (1998).
- <sup>73</sup>J.-Y. Fang and S. Hammes-Schiffer, *J. Phys. Chem. A* **103**, 9399 (1999).
- <sup>74</sup>J. E. Subotnik, *J. Chem. Phys.* **132**, 134112 (2010).
- <sup>75</sup>K. Wong and P. Rossky, *J. Chem. Phys.* **116**, 8418 (2002).
- <sup>76</sup>P. Attard, *J. Chem. Phys.* **130**, 194113 (2009).